Proceedings of the IASS 2024 Symposium
Redefining the Art of Structural Design
August 26-30, 2024, Zurich Switzerland
Philippe Block, Giulia Boller, Catherine DeWolf,
Jacqueline Pauli, Walter Kaufmann (eds.)

Post-analysis of Wisdome Stockholm: a comparative study of building model versus constructed geometry

Evy Laura SLABBINCK*, Stefan RICK[b], Moritz NIEBLER[a], David RIGGENBACH[c]

*Design-to-Production
Seestrasse 78, 8703 Erlenbach, Switzerland
slabbinck@designtoproduction.com

[a] Design-to-Production, Seestrasse 78, 8703 Erlenbach, Switzerland
[b] SJB Kempter Fitze, Zürcherstrasse 239, 8500 Frauenfeld, Switzerland
[c] Blumer-Lehmann AG, Erlenhof, 9200 Gossau, Switzerland

Abstract

In December 2023, Wisdome Stockholm, an innovative 47-metre timber gridshell roof, was inaugurated at Sweden's National Museum of Science and Technology. Employing on-site bending of laminated veneer lumber (LVL) lamellae. This paper presents a post-analysis of Wisdome Stockholm to evaluate the accuracy of its building model against the constructed geometry. The study compares the 3D-building model with the actual roof geometry, examines the non-developable nature of the beam geometry comprising LVL lamellae, and analyses internal stress calculations of the timber gridshell. This paper aims to enhance our understanding of the accuracy of architectural and structural models in complex bent-on-site free-form timber structures. The insights derived are intended to be instrumental for future timber gridshell constructions, guiding the refinement of methodologies and models in the pursuit of enhanced precision and reliability in architectural and structural design.

Keywords: post-analysis, timber gridshell, collaboration, interdisciplinary solutions, wood-only construction, free-form structures

1. Introduction

The 'Wisdome Stockholm' project represents advancements and exemplifies the potential in sustainable timber architecture, designed by Elding Oscarson in collaboration with various stakeholders to extend the Tekniska Museet in Stockholm, Sweden. The innovative structure features a 25x47-metre free-form timber roof constructed from 2,650 31-millimetre-thick CNC-cut spruce laminated-veneer-lumber (LVL) lamellae, sponsored by Stora Enso. The meticulous 1.5-year planning phase reached its topping-out milestone in December 2022 and was opened to the public in December 2023. Construction employed glued pre-curved LVL beams for the falsework and bottom beam layer A, supporting bent-on-site layers B to E, each with five LVL lamellae (a to e), fastened by 3,500 dowels (Figure 1 and 2) and screws. The cross-section width of the beam layers tapers from 500 to 380 millimetres, changing with each lamella. To counteract the roofs' horizontal thrust, columns required to be pretensioned.

This approach, necessitated by material constraints by the sponsor, optimised truck load efficiency and avoided costly doubly curved glulam blank fabrication. The collaborative efforts of architects, engineers, contractors, and consultants were crucial in achieving this innovative construction. Upon completion, a post-analysis by the timber team was conducted to drive advancements in timber construction aiming to advance our understanding of architectural and structural model accuracy in complex free-form structures. This paper builds on the previous work by Slabbinck *et al.* [1], providing a more in-depth explanation of the integrative approach to Wisdome Stockholm and additional details.

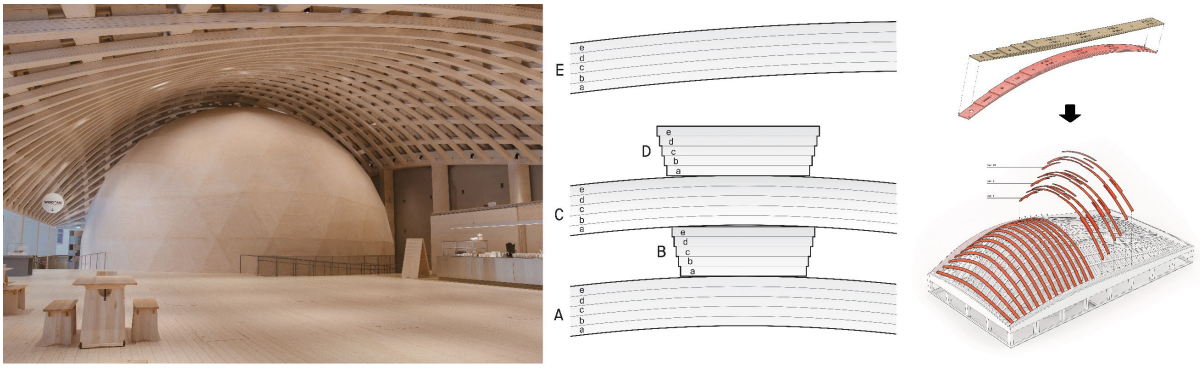

Figure 1: Left: Wisdome Stockholm [Focus Format, Gabriel Huber, Blumer Lehmann] Other: beam and lamella layer overview; bent-on-site flat-packed timber gridshell [Design-to-Production]

2. Navigating complexity: digital planning and structural analysis methodologies

During the digital planning phase, the Design-to-Production (D2P) master model serves as both the target model for on-site construction, the input model for structural processes, subject to geometric modifications due to column pretensioning and temporary support, as well as the model where production data is extracted and delivered to the various fabricators. The post-analysis focuses on three main aspects: (1) a comparison between the structural 3D-building model and the scanned geometry of the constructed roof, (2) an examination of the beam geometry of the lamellae, considering their non-developable nature and quantifying the error introduced during unrolling within permissible tolerances, and (3) an in-depth analysis of the internal stress calculations for the timber gridshell lamellae, comparing different modelling and calculation approaches and benchmarking the large deformation simulations conducted for the Wisdome Stockholm.

2.1. Digital planning process

The role of digital planning in the creation of complex free-form shell structures is key, demanding advanced geometry and modelling expertise. Employing the well-established agile D2P process [2] was instrumental in leveraging the full potential of digital fabrication and ensuring the project's timely and budget-conscious completion. This included delivery an early bill of quantities (BoQ) for material procurement and precise 5-axis fabrication data for machining. Furthermore, the rationalisation of recurring building elements to a selective few type facilitated mass production and streamlined logistics. The "unrolling" of lamellae, inclusive of their complex details, was automated through parametric 3D-modelling, simulating their elastic material behaviour [3], further discussed in 5.2.

2.2. Structural analysis process

The structural model of Wisdome Stockholm, like any other structural model, serves as an approximation of reality. Primarily, it aims to ensure the safety of the building and its occupants while striving to closely emulate real-world conditions to achieve structural efficiency. The complexity of obtaining this approximation results in a model filled with numerous elements and data. Additionally, the project introduces an additional layer of complexity due to its experimental approach of initially employing flat elements and bending them on-site. Furthermore, the beams consist of five individual lamellae. Unlike conventionally glued beams where the entire structure's moment of inertia can be calculated from the collective layers as one beam, in this instance, due to their disconnected nature, this cumulative calculation is not feasible and needs to be modelled and calculated as single lamellae.

3. Precision and tolerance management

In the design of timber structures, it is imperative to account for tolerances due to the material's hygroscopic, porous, and orthotropic nature, which renders it sensitive to variations in humidity across three dimensions [4]. Consequently, tolerances throughout the design-to-installation process of the building are meticulously predetermined to ensure precise fitting of the elements on-site.

During the digital planning process, model tolerances were set at 0.000001 millimetres to maintain high accuracy standards and ensure compatibility with other software platforms like Cadwork. The 31-millimetre thick raw LVL boards provided by Stora Enso, with a standard thickness tolerance of +/- two millimetres, were calibrated, indicating a refined tolerance of +/- 0.3 millimetres. However, transportation and assembly may influence this tolerance due to variations in the material's moisture content due to fluctuations in temperature and relative humidity [5].

The machine tolerances, specifically from TW-Mill Technowood, are minimal, typically within the range of +/- 0.1 millimetre. Nonetheless, deviations can occur during machining, especially when clamping components. For instance, in the case of clamping layer A, the assembly was executed using a jig that lacked full rigidity. Considering the cumulative impact of these variables, the deviation is estimated to fall between +/- three and five millimetres. This was accounted for during the design phase, processing interface points with adjacent components to reduce tolerance to an acceptable range of +/- 1.5 millimetres.

For assembly, undersize tolerances were set at 0.5 millimetres for non-load-bearing elements and a precise 0 millimetres for load-bearing components. Load-bearing accuracy was verified during the mock-up phase, leveraging the conical dowel geometry to compensate for manufacturing tolerances. This compensation led to a tight fit for load-transfer at contact points. Non-load-bearing surfaces were designed with a 0.5-millimetre clearance on both sides to accommodate manufacturing tolerances and wood's hygroscopic variating properties without increasing installation force. Additionally, a classical timber engineering approach was adopted for the connection between edge beams and columns, incorporating a one to two millimetre 'shadow gap' tolerance and oversize.

4. Comparison of the 3D building model with constructed geometry

4.1. Overview of the building model and taking reality into consideration

In Chapter 3, tolerances are examined, with the building model achieving an accuracy of 0.000001 millimetres. The model incorporates logistics, assembly, installation, fabrication, structural engineering, and material considerations to ensure realistic and efficient construction. Lamella segmentation is based on logistic constraints and engagement feasibility. Coordination is required for engagement over multiple dowels, with an engagement angle analysis and structural evaluation were conducted. Material constraints for maximal torsion and bending were analysed for each lamella, leading to geometry optimisation. Additional optimisation parameters included the minimum sloping angle of the roof shingles. Different tolerances were integrated to ensure optimal load transfer of the tight-fit dowels for shear forces and ease of assembly. Dowel rationalisation maximised standardisation and reduced material waste (Figure 2). The resulting dowel types were optimised for fabrication to reduce machining and finishing time. Additionally, early establishment of a logical naming and numbering system for each component streamlined logistics. Coordinating the logistics of 2,650 lamellae made from two different materials (LVL-S and -X) with varying visible qualities necessitated meticulous planning. The digital planning process optimised nesting groups and production batches for timely site delivery (Figure 2).

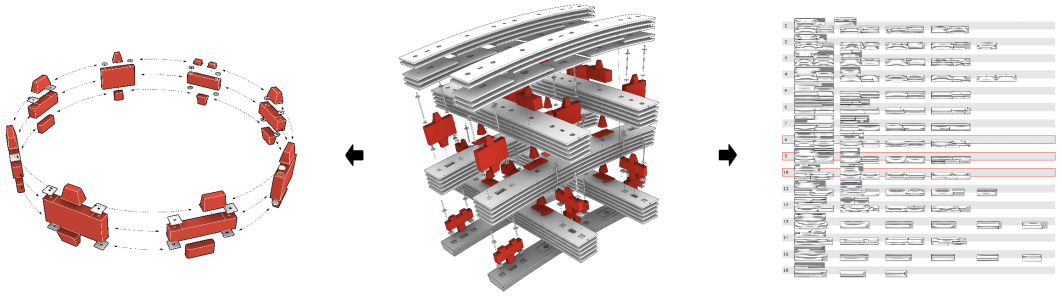

Figure 2: Dowel rationalization; detailed roof build-up; nesting groups for production [Design-to-Production]

Post-model, coordinating production batches involved aligning raw material delivery, lamella fabrication, and loading sequence aligned with assembly orders. On-site beams needed precise stacking and alignment for efficient hoisting. For assembly, a temporary structure was planned to position the initial beam layer A accurately. Additionally, a flat system scaffold was employed to ensure accessibility and work safety for assembly personnel. The construction site was weather protected by a site-cover-tent, including covering the delivery and buffer-storage zone for materials.

4.2. Scanning process

Upon completion, the building was measured on-site and compared to deformation predictions calculated from a structural model (Graph 1). Vertical deviations were determined by measuring primarily defined control points on the roof using a tachymeter, while horizontal deflections were measured along the edge beam with a taut string. Measurements were taken at three different structural states:

a. Before pretensioning the columns (prior to tensioning the Dywidag anchors in the supports)
b. After pretensioning the columns
c. After removal of the temporary support

The structural model used for comparison considered the exact on-site boundary conditions. For situations a and b, all installed members were considered (excluding shear and tension panels, and layer E [1]), with similar load case (deadload, pretension of the lamellae, and no creeping effects), situation b had additional pretension of the Dywidag anchors. For situation c, all structural members were installed (including shear and tension panels, and layer E [1]), with the same load case as situation b. Rafters, rafter panels, and additional roof cladding were not considered in any situation [1].

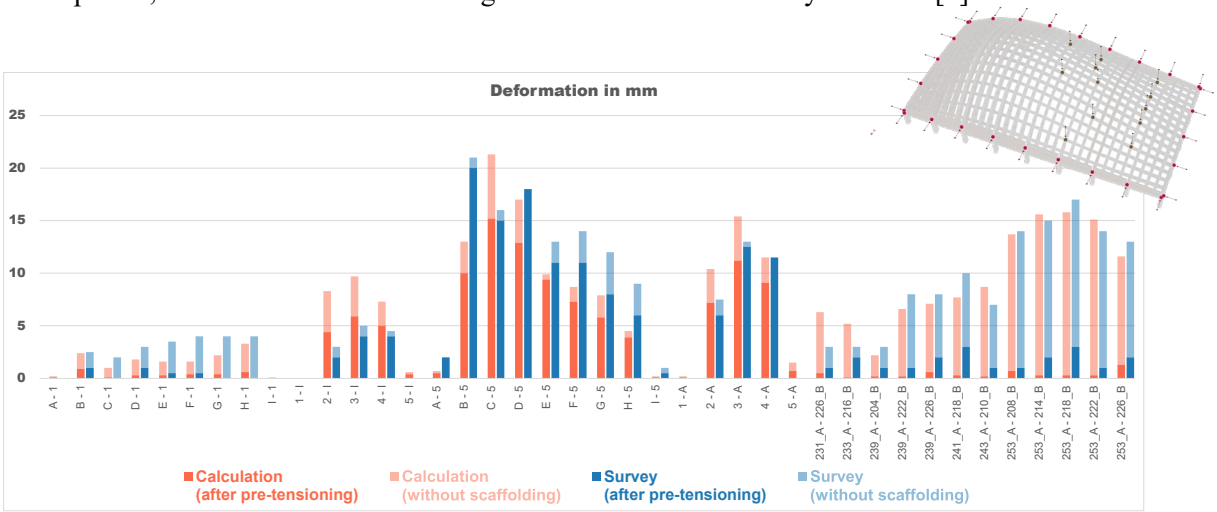

Graph 1: Overview deformations of the on-site measurement and structural model calculations

4.3. Accuracy of the scanning

The tachymeter's tolerance is predicted to be less than one millimetre. However, accuracy largely depends on the precision of holding the measuring mirror, resulting in an expected deviation range of two to three millimetres. For measurements using the taut string, inaccuracies are estimated to be around one millimetre.

4.4. Implications and findings

The deformations observed in the structural model align closely with those measured on-site. When comparing total deformations post-pretension and without temporary supports (situation c), a maximum difference of eight millimetres was identified between the structural model and on-site measurements. Considering tolerances, the difference ratio ranges from 5 to 11 millimetres, averaging 2 millimetres

without tolerances. Hence, it can be confidently concluded that the on-site deformations aligned with the predictions from the structural model.

Additionally, the moisture content of the lamellae were measured. The LVL was manufactured with a low moisture content of approximately 8 to 9 percent. However, due to unsealed ground in the storage-buffer zone and higher-than-expected humidity inside the tent, noticeable swelling of the LVL occurred. This led to a significantly higher force requirement for the joining processes than initially anticipated.

5. Beam geometry analysis

5.1. Geometrical approach lamella surface

As outlined in the introduction, the beams consist of LVL-lamellae that are bent and twisted on-site, resulting in elastically deformed elements, commonly known as bending-active elements [6]. Lienhard [6] categorised bending-active structures into three design methodologies: the behaviour-based approach, the geometry-based approach, and the integral approach. These methodologies can be classified as either bottom-up, such as empirical or numerical methods through form-finding, or top-down, relying on analytical geometry using mathematical equations like elastica-ruled surfaces [7]. The majority of contemporary designs for bending-active structures and elastic gridshells utilise numerical form-finding to determine the equilibrium shape in three-dimensional space [8][9]. For continuous bending-active plates, La Magna *et al.* [10] introduced form-conversion, a top-down approach that begins with a meticulously selected target geometry and develops it into single-curved developable surfaces, resulting in near-zero Gaussian curvature. Conversely, the bottom-up or form-conversion approach aims to create a 3D surface that can be unrolled onto a plane without distortion.

In the Wisdome Stockholm project, the reference geometry neither underwent form-finding nor represented a developable surface. Moreover, the lamellae derived from the beam-axis grid on this reference surface did not align with the principal curvature lines, leading to a non-developable nature of the lamella surfaces. While a Gaussian curvature analysis revealed only a minimal value, rather than zero—indicative of an exact developable surface—it suggests that quasi-developable surfaces were employed for the lamellae in this project [11]. The driver for defining the beam curve network were primarily design-driven, aiming for an even distribution across the surface that aligned with the design intent while considering material constraints. This approach maintained the torsional angle and bending radius of the lamellae within predetermined limits. The resulting lamella surface along the reference surface is a ruled surface (Figure 3), allowing a line to be drawn from every point on that surface that lies within it [12]. Furthermore, the mid-surfaces of the lamellae—i.e., the centre surfaces of the lamellae—are NURBS surfaces with a degree of 3 in the U-direction, conforming to the free-form reference surface, and a degree of 1 in the V-direction. These degrees underscore the ruled nature of the surface and accommodates the material constraints of the plates, resulting in surfaces with double curvature.

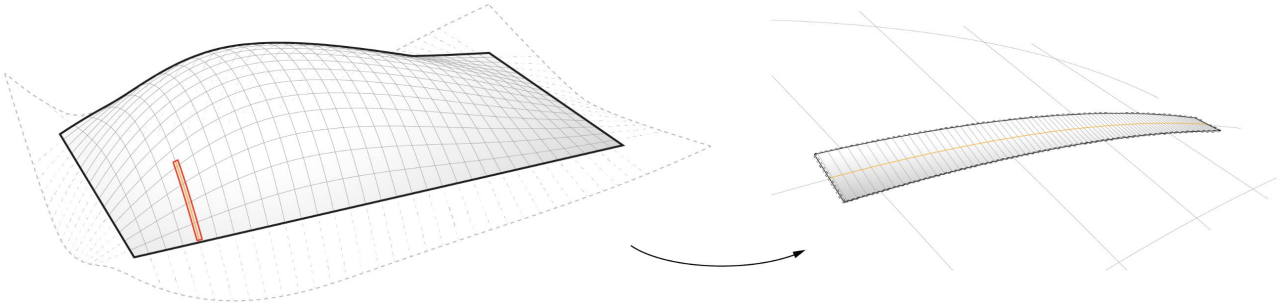

Figure 3: Reference surface with beam curve network; mid-surface of the lamella

5.2. Unrolling process and deviation control in lamella geometry

The process of generating the geometry for the thin lamellae—referred to as 'unrolling' from curved to flat—was conducted through a two-step approach. These steps were executed individually due to project scheduling constraints and the lead times required for material procurement [3].

In the first step, the spatial lamellae (3D) were planned according to a conventional method based on a reference surface, with a beam grid network employed to generate single ruled lamella surfaces that are locally tangent to the reference surface. As previously mentioned, non-developable surfaces cannot be accurately unrolled mathematically. For the unrolling process in Rhinoceros3D, the CAD software utilised in this project, the API-based function relies on intricate transformation matrices that account for material stretching and shrinking [13]. These unrolled lamellae contours were produced without detailed construction information and were subsequently nested onto raw material sheet boards for material procurement.

In the subsequent step, the unrolling of detailed geometry operations, such as cutters and drilling axes, for the production model were mapped onto the pre-existing unrolled lamellae. Prior to this, a 'flat sister lamella' was generated from the mid-surface of the lamellae using the methodology from the initial step and was incorporated into the process. The unrolling of detailing follows a three-step approach. Firstly, local coordinate systems and detail planes, complete with metadata regarding their relative positions, were unrolled along the mid-surface lamella. This was followed by remapping all details onto the sister lamella, allowing for the uniform application of the same unrolling routine across all operations, including drillings, saw cuts, pockets, and block instances with intricate cutter geometries. This process is conducted in a serialised manner, enabling simultaneous detailing across a single lamella. Finally, the geometry and metadata are deserialized back into a local coordinate system relative to the flat mid-surface [3]. Due to the non-developable nature and double curvature of the surface, deviations from the original surface were introduced during the unrolling process. These deviations arose not only from the function that accounts for material characteristics but also from the unrolling of the coordinate systems themselves. Due to the curvature and the unrolling of points along the surface, a deviation in relative position was anticipated. These expected deviations were carefully managed and controlled during the design process.

To control both induced deviations, a control algorithm was implemented in the process. The focus of this paper will exclusively be on the deviation resulting from unrolling the mid-surface. To accurately quantify and assess the induced deviation between the unrolled surface and the original 3D surface, consistent and evaluable measurements were required. Given the non-developable nature of the 3D surface, and the consequent different parametrisation of the unrolled NURBS surface, a control-point network evaluation was deemed unsuitable. The chosen approach involved comparing the lengths of the four surface edges. Each edge length from the 3D surface was compared to the corresponding length of the unrolled surface edge, with a negative value indicating shrinkage and a positive value indicating stretching. Throughout the unrolling process, the control algorithm ran in the background for the sister lamella surfaces, and deviations were monitored against a fraction of the machine tolerances, as detailed in chapter 3. If the deviation exceeded the set bounds, a warning was triggered. However, logging of these deviations was not conducted during the planning phase, as no unrolled surface surpassed the fabrication tolerance.

5.3. Quantitative analysis of deviations and correlations in lamellae

For the post-analysis, a quantification of the induced deviations was conducted. A sample set of 655 lamellae from layer C was analysed and documented, drawn from a total of 2,650 lamellae. The same control algorithm was employed to measure the deviation in edge lengths, and additionally, the deviation in surface area was also compared. To gain a deeper understanding of the lamellae context, the bending radii and torsional angles for each lamella were also analysed. For a more comprehensive overview, only the maximum deviation value among the four edges was considered in the quantification.

The results indicate that the edge deviation ranges from -1.63 to 0.45 µm, as shown in Graph 2. Additionally, the area deviation ranges between -585 to 0 mm^2, equivalent to the area of a two-euro coin, as depicted in Graph 2. The consistent negative values for area deviation suggest that all unrolled lamellae in the sample set are marginally smaller than the original 3D lamellae. Contrary to the positive edge deviation values, which initially suggested a positive area deviation, keeping in mind the values only represent the maximum deviation among the four edges of each lamella. This discrepancy confirms shrinkage, as evidenced by one concave and one long convex edge curve, with one edge shrinking and

the other stretching. To further illustrate the correlation between the number of deviations, see Graph 3 and 4.

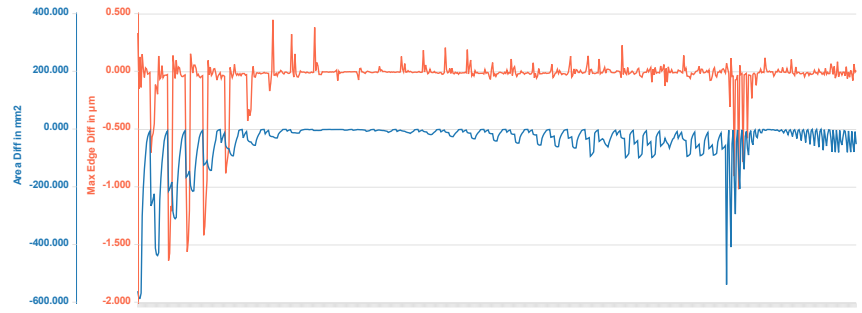

Graph 2: Max. edge difference in [µm] and area difference in [mm^2]

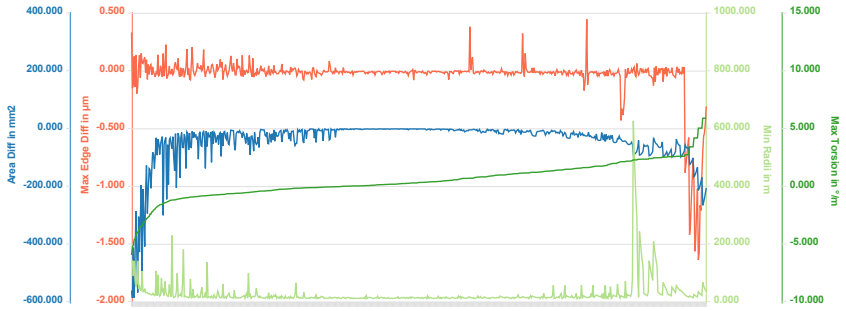

Graph 3: Max. edge difference in [µm] and area difference in [mm^2] with max. torsion [°/m] and min. bending radii [m] - sorted by amount of torsion

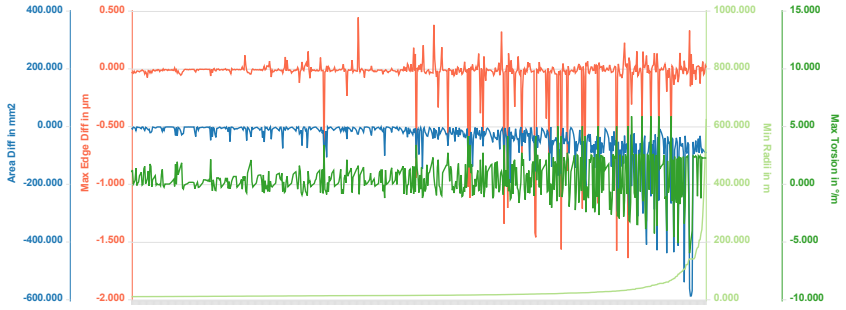

Graph 4: Max. edge difference in [µm] and area difference in [mm^2] with max. torsion [°/m] and min. bending Radii [m] - sorted by amount of bending radii

5.4. Discussion on quantitative analysis

Graph 2 demonstrates that the edge deviation ranging from -1.63 to 0.45 µm falls well below the machining tolerance of 0.1 mm, as specified in chapter 3. Additionally, it illustrates a direct correlation between edge deviation and area deviation. Furthermore, the anticipated outcome—that lamellae not subjected to torsion would exhibit no deviation, resulting in a developable surface—is corroborated by the results presented in Graph 3. This indicates that torsion induces a greater deviation than lamellae primarily subjected to bending, as evidenced by an increase in Gaussian curvature.

Graphs 3 and 4 reveal that areas with smaller bending radii, indicative of greater bending curvature, exhibit less torsion, and vice versa. This phenomenon can be attributed to surface geometry; towards the edge of the roof where higher torsion is prevalent, there is less bending of the lamellae. Conversely, in areas with higher curvature, such as the peak of the roof, torsion is minimal.

6. Internal stress calculation of the lamellae

6.1. Modelling and calculation process

Within structural analysis, the computation and simulation of internal stresses represent a critical component. Given the initial planar configuration of the elements, internal stresses are induced in the final structural geometry. Performing simulations for all 2,186 lamellae (layer B to E) transitioning from a planar state to their 3D configurations would be computationally inefficient and imprudent. The structural analysis process is an extension of the digital planning phase, utilising the master model as primary input. To accurately account for torsional and bending stresses within the structural model, a reverse engineering approach was employed. Finite element analysis was conducted using Dlubal, specifically employing RSTAB. Notably, the use of NURBS surfaces was not possible, necessitating the polygonization of the axis of each lamella. Furthermore, each structural member necessitates a localised axis system and interconnections (links) between lamellar axes to facilitate load transfer between adjacent elements. Utilising parametric design outputs, torsional angles and curvatures for each lamella in its 3D geometry at specified intervals were evaluated (Figure 4). The torsional moment was subsequently deduced from the torsional angle (angle of twist) for each segment. Using Excel, this torsional moment, coupled with the curvature value, was applied to the structure within RSTAB to deform the lamella to its 3D configuration. Thereafter, computations were executed in RSTAB with all imposed loads. This analytical approach is essential not only for assessing internal stresses to determine material adequacy, particularly under external loading conditions, but also for calculating the connection resistances against lamellar recoil.

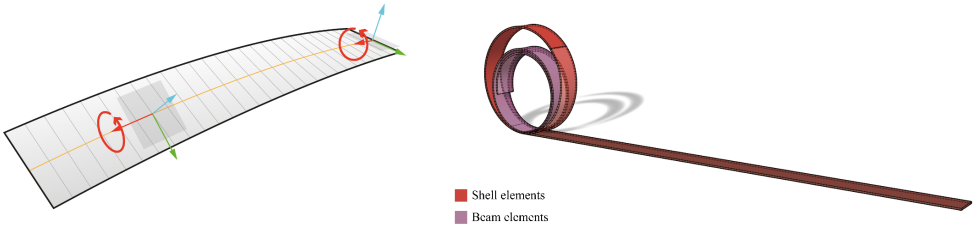

Figure 4: Left: Angle of twist and local axis system in the lamella; Right: Sofistik benchmark test in Dlubal

During the Wisdome Stockholm, a comparative analysis was conducted between manual calculations and Finite Element Analysis (FEA) simulations. The input parameters for the LVL included a shear modulus (G) of 600 N/mm^2, a cross-sectional dimension of 31 mm in height and 380 mm in width, a torsional moment (M_T) of 0.039 kNm, and a test length of 1 metre. The objective was to ascertain whether utilising the M_T as an input parameter would yield consistent torsional angles (φ) in both methods.

$$I_T = c_1 \cdot b \cdot h^3 = 0.316201 \cdot 380 \cdot 31^3 = 3{,}579{,}587 mm^4 \quad (1)$$

$$\varphi = \frac{M_T \cdot L}{G \cdot I_T} = \frac{39{,}000 Nmm \cdot 1{,}000 mm}{600 \frac{N}{mm^2} \cdot 3{,}579{,}587 mm^4} = 0.018157 rad = 18.2 mrad \quad (2)$$

An evaluation was conducted utilising both beam elements in Dlubal RSTAB 8 and shell elements in Dlubal RFEM 5 (Figure 5). In the shell element analysis, applying a torsional moment to a single node was deemed inaccurate; hence, the torsional moment was redistributed as a couple of forces. Both computational methods yielded consistent torsional angles when subjected to identical torsional moments. While a comparative analysis of FE software tailored for bending-active structures, particularly for simulating lamellae, falls outside the scope of this paper, it's noteworthy that caution is warranted when interpreting results due to the uncommon nature of large deformation analysis, as highlighted by Lienhard [6]. To address this, the Sofistik benchmark test no. 8 [14], focusing on the large deflection of cantilever beams II, was executed, as depicted in Figure 4 on the right, demonstrating convergence in both beam and shell element simulations.

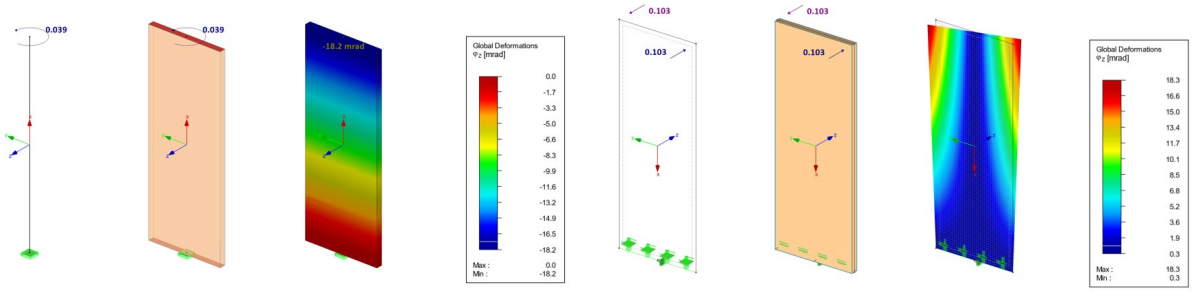

Figure 5: Left: the results in RSTAB 8; Right: the result in RFEM 5

6.2. Simulation of sample lamella in bending and torsion

A representative lamella sample was selected for post-analysis, involving simulations in RFEM and RSTAB compared with the target geometry in the master model. Specifically, the chosen sample lamella pertains to beam layer C and represents the third lamella layer c. The initial flat lamella, derived from the digital planning process as detailed in chapter 5, serves as the base geometry. To simulate the target 3D geometry, nodal deformations are applied to the flat lamella, considering solely z-direction displacements to avoid constraints and unrealistic phenomena like bending around the strong axis. The simulations are executed using third-order non-linear analysis, i.e. large deformation analysis, with small incremental load steps set at 0.1. To evaluate the fidelity of the deformed geometry relative to the target geometry, the final node coordinates from the FEA simulations are extracted and superimposed onto the target model, as illustrated in Figure 6. Additionally, the bending stresses are compared to the Wisdome Stockholm structural approach, using the reversed- engineering approach, see chapter 6.1.

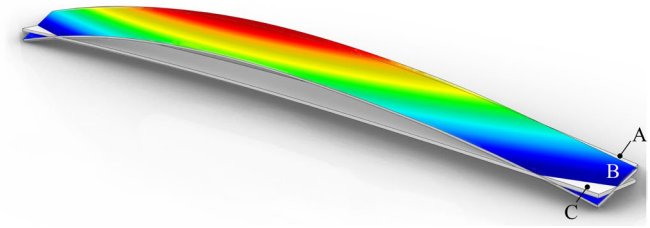

Figure 6: Deformation comparison: A- target model, B- RFEM results and C- initial flat lamella

6.3. Comparative analysis of modelling approaches and insights to internal stresses

The utilisation of the cross-section for bending stresses in the fibre direction and shear stresses between beam and shell analyses are comparable. Bending stresses reach up until 45% of the maximum allowable 50 N/mm^2, while shear stresses approach 69% of the permissible 2.3 N/mm^2. Differences in geometry between the target and deformed lamella in FEA stem from induced displacements solely in the z-direction yet remain within acceptable limits. The bending and shear stress comparison between the Wisdome Stokholm approach and the post-analysis in the previous paragraph shows the same utilisation rate for the lamella. The decision to utilise beam elements in the Wisdome Stockholm analysis is attributed to their simplicity, resulting in computational efficiency. Beam elements require fewer nodes and degrees of freedom, expediting meshing and yielding faster solution times, especially for large-scale structures. Additionally, beam elements offer stability, reduced susceptibility to numerical instabilities, and facilitate straightforward result interpretation and visualisation. Furthermore, the load case analysis of Wisdome Stockholm was also examined without considering internal stresses. While internal stresses can enhance the structure's stability and rigidity, their effects diminish over time [15].

7. Conclusion

In this study, we examined the precision of architectural and structural models for the Wisdome Stockholm, a complex free-form bent-on-site timber gridshell construction. The collaborative efforts of the architect and the timber team resulted in an innovative approach influenced by material constraints.

This study emphasises the importance of post-evaluations, especially for novel construction methods that rely on assumptions, to provide valuable insights for future projects. Our findings indicate that on-site deformations closely matched the predictions from the structural model. Deviations observed during unrolling were well within acceptable machining tolerances. Additionally, the structural calculation process, which involved applying torsion angles and curvature values to a bent geometry using beam elements in FEA, proved to be a successful approach for simulating structures with numerous elements that are bent-on-site. In summary, the study underscores the importance of meticulous planning, collaboration, and keeping tolerances in mind from early design stages.

Acknowledgements

The Wisdome Stockholm, designed by Elding Oscarson and commissioned by Tekniska Museet, is a collaboration between different companies: Florian Kosche, Stora Enso, SJB Kempter Fitze, Création Holz, Design-to-Production, Blumer-Lehmann, Roth, Balteschwiler, Gebhard Müller, Olijbe and Oberholzer.

References

[1] E.L. Slabbinck, H. Blumer, S. Rick, D. Riggenbach, M. Antemann and F. Scheurer, "Integrative approach to a timber gridshell formed on-site," *Proceedings of the IASS Annual Symposium,* 2023.

[2] F. Scheurer, H. Stehling, F. Tschümperlin and M. Antemann, "Design for Assembly –Digital Prefabrication of Complex Timber Structures," *Proceedings of the IASS Annual Symposium,* 2013.

[3] M. Niebler, S. Usai, M. Antemann, F. Scheurer and E. Slabbinck, "Bent-on-site flat-pack delivery of a timber shell," *Advances in Architectural Geometry*, K. Dörfler, J. Knippers, A. Menges, S. Parascho, H.Pottmann and T. Wortmann, Eds., Berlin, Boston: De Gruyter, 2023, pp. 69-82.

[4] D. Tong, S. Brown, H. Yin, D. Corr, E. Landis, G. Di Luzio and G. Cusatis, "Orthotorpic hygroscopic behavior of mass timber: theory, compution, and experimental validation," *Materials and Structures*, vol. 56, no 6, 2023.

[5] P. Dietsch, S. Franke, B. Franke, A. Gamper and S. Winter, "Methods to determine wood moisture content and their applicability in monitoring concepts," *Journal of Civil Structural Health Monitoring*, vol. 5, pp. 115-127, 2015.

[6] J. Lienhard, "Bending-Active Structures," Ph.D. dissertation, University of Stuttgart, 2014.

[7] T. Lee and Y.M. Xie, "From ruled surfaces to elastica-ruled surfaces: new possibilities for creating architectural forms," *Journal of Intern. Association for Shell and Spatial Structures*, vol. 62, no. 4, pp. 271-281, 2021.

[8] Y. Sakai, M. Ohsaki and S. Adriaenssens, "A 3-dimensional elastic beam model for form-finding of bending-active gridshells," *Intern. Journal of Solids and Structures*, vol. 193, pp. 328-337, 2020.

[9] S. Kookalani, S. Nyunn and S. Xiang, "Form-finding of lifting self-forming GFRP elastic gridshells based on machine learning interpretaility methods," *Structural Engineering and Mechanics*, vol. 84, no. 5, pp. 605-618, 2022.

[10] R. La Magna, S. Schleicher and J. Knippers, "Bending-active Plates, " *Advances in Architectural geometry*, S. Adriaenssens, F. Gramazio, M. Kohler, A. Menges, M. Pauly, Eds., pp. 170- 186, 2016.

[11] F. Perez and J.A. Suarez, "Quasi-developable B-spline surfaces in ship hull design," *Computer aided design*, vol. 39, pp. 853-862, 2007.

[12] L. Piegl and W. Tiller, "Construction of Common Surfaces," in *The NURBS book. Monographs in Visual Communications*. Berlin, Heidelberg: Springer, 1995.

[13] McNeel, "UnrollSrf," McNeel documentation, 2024 [online]. Available: docs.mcneel.com/rhino/7/help/en-us/commands/unrollsrf.htm [Accessed April 06, 2024].

[14] Sofistik, "Benchmark Example No. 8," *Sofistik documentation*, 2023.

[15] E.L.M. Slabbinck, A. Koerner and J. Knippers, "Torsion as a design driver in plate-bending-active tensile strcutres," *Proceedings of the IASS Annual Symposium ,* 2017.